Robust Identification of Concealed Dangerous Substances by Spectral Correlation of Terahertz Transmission Images

Arthur D. van Rheenen and Magnus W. Haakestad, *Member, OSA*

***Abstract*—Terahertz images containing spectral information in each pixel are recorded in transmission mode using a fiber-coupled time-domain spectroscopy system. The images are acquired by mounting a sample holder on an x–y stage, which is stepped across the beam in the two transverse directions, while the transmitted THz waveform is captured. The materials under investigation consist of uncovered and hidden samples of an explosive (RDX) and simulants (lactose and tartaric acid). Spectral angle mapping is used to identify the materials in the Terahertz images by comparing the spectrum in each pixel with a library of reference spectra for the different materials. We test the performance of several spectral characteristics derived from the measured transmission spectra. Robustness is studied by investigating the Receiver-Operating-Characteristics (ROCs). The ROCs are used to find which of the spectral characteristics is most robust to different sample preparation conditions, without the need for extensive pre-treatment of the data, such as baseline correction. Simple theoretical considerations are used to support the experimental results.**

***Index Terms*—Terahertz, spectroscopy, imaging.**

I. Introduction

ONE of the most promising applications of Terahertz spectroscopy is detection and identification of dangerous and/or illegal substances [1]. The ability to penetrate common materials, such as plastics, cloth, and cardboard, allows for identification of these substances, even when they are concealed. We here investigate the robustness of a simple spectral recognition method known as spectral angle mapping (SAM) [2]. In SAM the measured spectral characteristic of each pixel in the THz image is compared with a library of spectral characteristics by representing the characteristic as a vector and calculating the dot product, yielding the spectral correlation. We test several characteristics derived from the measured transmission spectra. Robustness is studied by investigating the Receiver-Operating-Characteristics (ROCs). The ROCs are generated by sweeping the identification (spectral correlation) threshold from -1 to 1 and counting the fraction of true-positive and false-positive pixels in the THz image. Preliminary results of this work have previously been presented in Ref. [3].

The combination of imaging and spectroscopy in security applications has the advantage of both being able to detect objects with a suspected shape as well identifying possibly harmful or illegal substances. THz imaging and a number of applications are reviewed in Ref. [4]. In this work the imaging capability is used to gather many spectra of the targets and the emphasis is on the spectral analysis. The object recognition is left to image processors at this stage. The issue of spectral identification is not new and has been used in for instance far-infrared Fourier transform (FTIR) spectroscopy. Localizing an absorption peak is relatively straight forward when the line is narrow, a common situation for FTIR spectra of gases. THz spectra of common simulants and explosives have rather broad peaks making it harder to pin down peak locations and hence identify substances. The literature on THz spectroscopy is growing, a selection of references are listed in Refs. [5]–[18]. The identification process is generally a question of matching a library spectrum to a measured spectrum and detection is declared if, in some metric, a threshold is exceeded. As a first cut at viewing the identification process one can look at it as a two-dimensional space with the different metrics (ways to compare spectra) along one axis and the spectral characteristics (which processed form of the raw spectrum) along the second axis. Common methods include principal component analysis (PCA) and spectral angle mapping (SAM) [5], [7], [9], [14], although also other methods have been used [12]. As to what to compare, there are several options, the raw spectrum, the raw spectrum normalized by a reference spectrum (transmission coefficient), and the absorbance. In addition, some groups apply preprocessing to their spectrum: removing water vapor lines and background scattering. Some authors pointed out that application of THz spectroscopy to security issues is not without difficulties [16]–[18]. It is the aim of this paper to quantify the spectral identification process by comparing several approaches and studying their false alarm rates.

In this work we have made several choices. (i) As a metric we chose SAM because of its simplicity and its intuitive nature. No extensive training of the algorithm is required, only a single library spectrum suffices. (ii) Preprocessing is limited to windowing of the time-domain signals. Water vapor lines and background scattering are not removed to allow for more realistic performance comparison. (iii) The different approaches are compared by studying their receiver operating characteristics (ROC), a simple visualization of their performance.

II. Theory

We will here describe how spectral angle mapping can be used to identify materials based on measured terahertz

A. D. van Rheenen and M. W. Haakestad are with the Norwegian Defence Research Establishment (FFI), P O Box 25, NO-2027 Kjeller, Norway (e-mail: Arthur-D.vanRheenen@ffi.no, Magnus-W.Haakestad@ffi.no).

DOI til publisert versjon/DOI to published version: 10.1109/TTHZ.2015.2400224

transmission spectra. From the scalar product of two vectors, $\mathbf{a}$ and $\mathbf{b}$, one can determine the cosine of the angle between them, according to the relation

$$\cos\theta = \frac{\mathbf{a}\cdot\mathbf{b}}{ab} \tag{1}$$

Similarly, from two spectral vectors, $\mathbf{S}$ and $\mathbf{S}_r$, one can form new spectral characteristics, $\mathbf{K}(\mathbf{S})$ and $\mathbf{K}(\mathbf{S}_r)$, where $\mathbf{K}$ is a vector function of the spectrum, and use the scalar product to find the cosine of the angle between them, which we denote as the spectral correlation; a number between -1 and 1, where 1 means perfect correlation. In this way one can compare a measured spectrum with a reference spectrum. The typical range of values of the spectral correlation depends strongly on which spectral characteristic $\mathbf{K}$ is used. However, a good spectral characteristic should yield a spectral correlation close to zero for two uncorrelated spectra and close to one for two similar spectra. It is thus important to choose a suitable spectral characteristic for optimal identification of the materials. The following expressions for $\mathbf{K}$ are tested and compared here:

- $\mathbf{K}_1 = \mathbf{S}$, where $\mathbf{S}$ is the raw spectrum (spectral amplitude).
- $\mathbf{K}_2 = -\ln\mathbf{T}$, where $T(f_i) = S(f_i)/S_{\text{air}}(f_i)$ and $\mathbf{S}_{\text{air}}$ is the spectrum of a measurement without sample, and f is the frequency.
- $\mathbf{K}_3 = -\frac{\mathrm{d}\ln\mathbf{T}}{\mathrm{d}f}$.

To estimate the performance of the spectral characteristics above, we consider the case where a sample is covered by a barrier material. As a simple approximation, we assume that the measured THz transmission spectrum is given by

$$S(f_i) = S_{\text{air}}(f_i)T_0\exp\left[-\alpha(f_i)L\right], \tag{2}$$

where T_0 is a constant attenuation factor, α is the absorption coefficient of the sample, and L is the sample thickness. The constant factor T_0 includes transmission through the barrier, as well as Fresnel reflection losses at the surfaces of the sample. A constant T_0 gives rise to a baseline in the absorbance $\mathbf{K}_2$. In Eq. (2), we have neglected multiple reflections from the sample and barrier materials, spectral characteristics of the barrier material, scattering from sample and barrier inhomogeneities, and noise.

From Eqs. (1)–(2) one can show that $\mathbf{K}_1$ gives a spectral correlation which is independent of a constant attenuation T_0 of the THz signal, but the spectral correlation is dependent on sample thickness. $\mathbf{K}_2$ gives the same spectral correlation for samples consisting of identical materials, with different sample thickness, as long as $T_0 = 1$. $\mathbf{K}_3$ gives the same spectral correlation for samples consisting of identical materials, with different sample thickness, for any constant value of T_0. For example, using Eq. (2), we obtain $\mathbf{T} = T_0\exp(-\alpha L)$ giving $\mathbf{K}_3 = \frac{\mathrm{d}\alpha}{\mathrm{d}f}L$. Thus

$$\frac{\mathbf{K}_3}{K_3} = \frac{\frac{\mathrm{d}\alpha}{\mathrm{d}f}}{\sqrt{\int\left(\frac{\mathrm{d}\alpha}{\mathrm{d}f}\right)^2\mathrm{d}f}}, \tag{3}$$

which is independent of L and T_0. The last point is especially important, as it avoids the need of baseline removal, as long as the baseline is frequency independent. A spectrally varying baseline, for example due to scattering, will have a negligible effect on spectral correlations based on $\mathbf{K}_3$, as long as the variation is sufficiently slow. Thus, based on these arguments, $\mathbf{K}_3$ is most robust to variations in measurement conditions.

To illustrate these considerations we generated an example spectrum with a single absorption line, the black curve in Fig. 1, and call this our library spectrum. The effect of a constant attenuation, possibly due to a concealing material, is modeled by the blue curve in the same figure. A thicker sample or a higher-concentration sample would yield a stronger absorption, represented by the red curve. To test the specificity

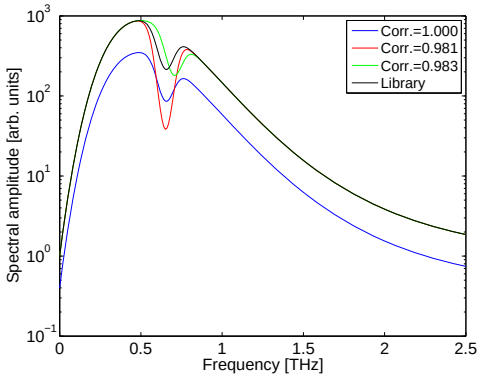

Fig. 1. Model spectra illustrating different spectral effects: black - standard model spectrum, blue - effect of constant attenuation, red - effect of stronger absorption, green - a different substance. The numbers in the legend show the spectral correlation with the library spectrum.

a model spectrum with the absorption center displaced by one line width is represented by the green curve in Fig. 1. The numbers in the legend indicate how well the different curves correlate with the library spectrum. Due to the comparatively small effect of the absorption line, the correlation is very close to 1 in all three cases.

Next, rather than using the raw spectrum, let us consider the absorbance, $\mathbf{K}_2$, see Fig. 2. It is obvious that the constant

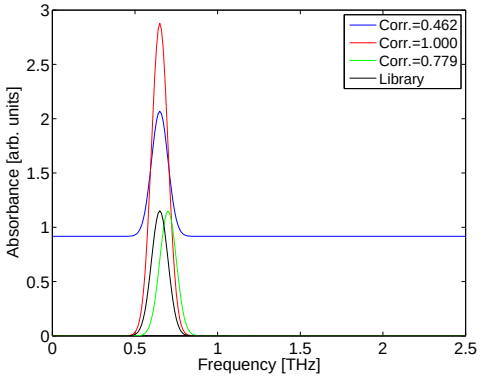

Fig. 2. Absorbance for the model spectra considered here, as well as their correlation with the library absorbance. See Fig. 1 for further explanation.

attenuation reduces the correlation significantly (0.46). The constant background needs to be removed from the spectra if this characteristic is to be used to identify substances. This characteristic is not sensitive (red - 1.00) to variations

Dette er en postprint-versjon/This is a postprint version.
DOI til publisert versjon/DOI to published version: 10.1109/TTHZ.2015.2400224

in sample thickness (absorption strength) and shows some specificity (green - 0.78).

Finally, consider the derivative of the absorbance. The curves are plotted in Fig. 3. This characteristic is neither

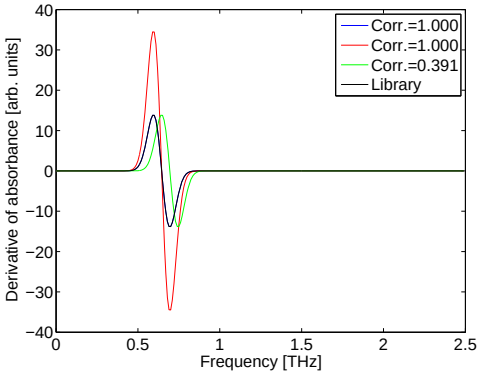

Fig. 3. Plot of the derivative of the absorbance for the model spectra considered here. The numbers show the correlation with the library spectrum. See Fig. 1 for further explanation.

sensitive to a constant attenuation nor to varying absorption strength: the correlation with the original spectrum is still perfect. In fact, it can be shown that even a slowly varying (polynomial of low order) background attenuation does not significantly hamper identification. In addition, this characteristic shows good specificity: the correlation for the model with the displaced absorption peak is significantly reduced (green - 0.39).

Based on this analysis the derivative of the absorbance appears to be the most promising spectral characteristic for identifying unknown spectra: It is both less sensitive to measurement conditions and more specific than the other characteristics.

III. Setup

The THz setup is based on a fiber-coupled time-domain spectroscopy system pumped by 100-fs pulses at 780 nm wavelength from a frequency-doubled Er-doped fiber laser [19]. THz images are acquired by mounting a sample holder on an x–y stage, which is scanned through the beam, with step size 1 mm, while the transmitted THz waveform is captured. In this way a THz spectrum (after Fourier transform) is acquired for each stage position (pixel). A schematic of the setup is shown in Fig. 4. The distance between the emitter and detector modules is 31 cm and the sample holder has room for 3×3 sample pellets, with diameter 32 mm and thickness up to 4.2 mm. Fig. 4 (inset) shows the labeling of the sample positions. Teflon (25 μm average particle size) was used as a binder material, which was mixed with tartaric acid, lactose, or RDX and then pressed into pellets using a 2 ton press in two minutes. The bottom row of the sample holder (position 7–9) was used for reference measurements, using a metal plate (position 7), no sample (position 8), and a pure Teflon sample (4 mm thickness, position 9). All measurements were performed in ambient air (21–26°C, 10–50% relative humidity). The signal at each position of the x–y stage (pixel)

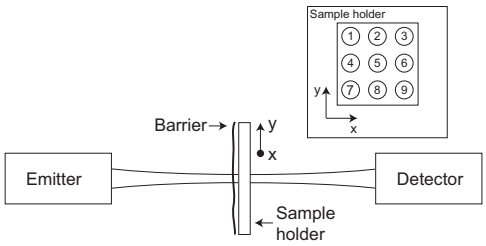

Fig. 4. Experimental setup. Two fiber-coupled photoconductive antennas act as emitter and detector modules, which are separated by 31 cm. A sample holder, with transverse dimensions 15×15 cm, is scanned through the THz-beam. Inset: Sample holder with labeling of samples indicated.

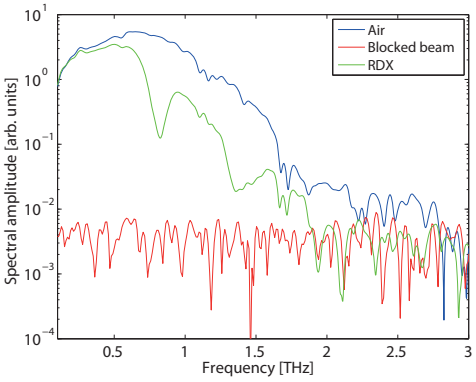

(a)

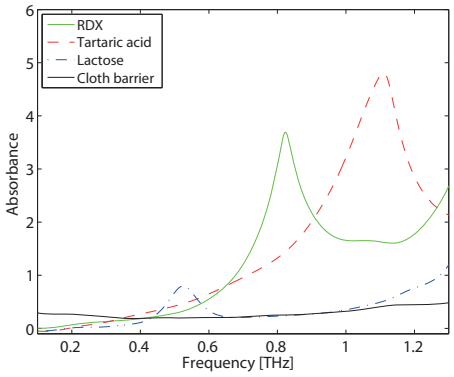

(b)

Fig. 5. (a) Reference spectra of air, blocked beam, and an RDX sample (after windowing of time-domain data). (b) Absorbance for the cloth barrier and reference samples containing RDX, tartaric acid, and lactose, respectively.

was measured with a time window of 60 ps and a scan speed of 1 ps/s, with a sample rate of 32 Hz.

Figure 5(a) shows reference spectra for an open beam (air) and blocked beam (noise). An example spectrum for a 10% (mass percent) RDX sample, with 3.5 mm thickness, is also shown in the figure. All spectra were calculated from the time-domain signals by first applying a Blackman-Harris window with 30 ps half-width, centered in time at the signal peak, and then calculating the Fourier transform (FFT). The reference spectra indicate a bandwidth of ∼2.5 THz and a peak signal-to-noise ratio (SNR) of ∼60 dB. Figure 5(b) shows the absorbance ($\mathbf{K}_2$) for samples containing RDX (10%, 3.5 mm thickness), tartaric acid (10%, 4.0 mm thickness), and lactose (10%, 4.2 mm thickness). These samples were

Dette er en postprint-versjon/This is a postprint version.
DOI til publisert versjon/DOI to published version: 10.1109/TTHZ.2015.2400224

used as reference samples in the spectral library. The part of the spectrum spanning the frequency range 0.1 to 1.3 THz was used in the correlation calculations, as the SNR is high in this frequency range (SNR>40 dB for an open beam). Although there are several water vapor absorption lines in this wavelength range [15], we did not perform any numerical removal of water lines in the data processing. The location of the water lines was used to verify the calibration of the frequency axis in our measurements. Also shown in Fig. 5(b) is the absorbance of the cloth barrier used in some of the experiments.

IV. Results

THz transmission measurements were carried out for samples containing tartaric acid, RDX, and lactose, and mixtures of two of these substances.

A. Uncovered samples

TABLE I
TARTARIC ACID SAMPLES FOR MEASUREMENTS WITHOUT BARRIER

Sample no.	Tartaric acid mass fraction	Total mass (g)	Thickness (mm)
1	5%	6.1	3.9
2	2%	6.3	4.0
3	1%	6.1	3.9
4	10%	3.1	2.3
5	10%	1.5	1.2
6	5% (unground)	6.2	4.0

Six tartaric acid samples were placed in the two top rows of the sample holder. The tartaric acid mass percent and sample thickness is shown in Table I. Sample no. 6 consisted of unground tartaric acid, while the tartaric acid was ground for the others. A reference spectrum for tartaric acid was measured using a 10% tartaric acid sample with 4 mm thickness, and is shown in Fig. 5(b).

Based on the measured terahertz transmission spectral image, a spectral correlation between each pixel and the reference sample was calculated. This assigns, in theory, a value between -1 and 1 to each pixel. Usually, amplitude or power spectra have only positive values for each frequency and SAM will then only yield correlation values ≥ 0. Derivatives of spectra may have negative values and negative correlation values are possible. All pixels containing tartaric acid (i.e. the same material as the reference sample) are labeled positive pixels, the remaining pixels being negative. One can classify a pixel by comparing its correlation value with a certain threshold. If the correlation value is larger than the threshold and the pixel is positive, the outcome is denoted as true positive. If, on the other hand, the correlation value is larger than the threshold and the pixel is negative, the outcome is denoted as false positive. The true positive rate (TPR) is the number of true positive pixels divided by the number of positive pixels and the false positive rate (FPR) is the number of false positive pixels divided by the number of false pixels. By stepping the threshold from -1 to 1 and calculating the TPR and FPR for the pixels in the image, we obtain the

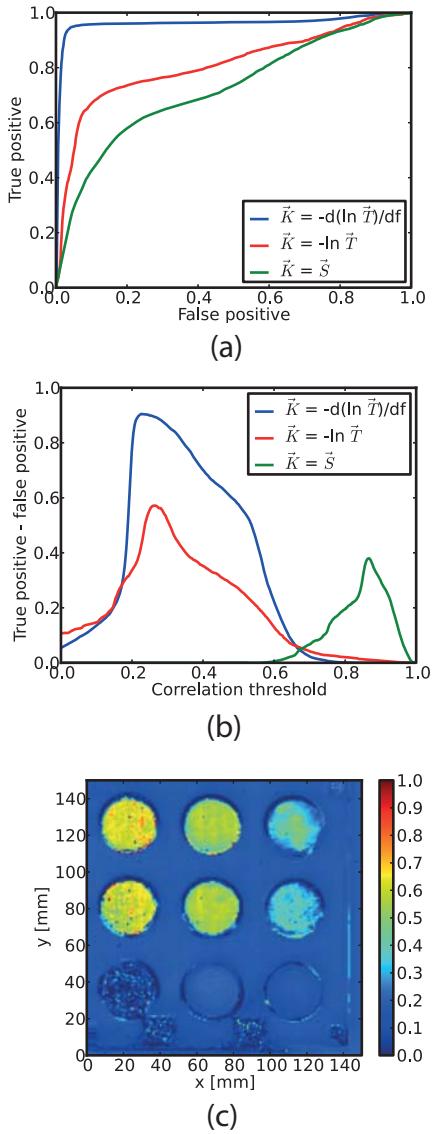

Fig. 6. Testing for tartaric acid, uncovered samples. (a) ROC curves for the three spectral characteristics for a THz image (transmission mode) of six tartaric acid samples and three reference samples. (b) Identifying the optimal identification threshold. (c) A spectral correlation image using the spectral characteristic $\mathbf{K}_3$.

ROC curves in Fig. 6(a). The ROC curves are based on the three spectral characteristics described in Sec. II. We observe from the ROC curves that the spectral characteristic $\mathbf{K}_3$ gives significantly better performance, compared to more common characteristics, such as the raw spectrum, $\mathbf{K}_1$, and the absorption spectrum, $\mathbf{K}_2$.

In practice, it will usually be desirable to operate in a regime where the fraction of false positive pixels is very low, while the fraction of true positive pixels is high, corresponding to the upper left corner of the ROC curves. The spectral correlation value corresponding to the upper left corner of the ROC curves is found by identifying the correlation threshold which give the largest difference between the fraction of true positive and false positive pixels (TPR$-$FPR). The results of this calculation are shown in Fig. 6(b). We observe from

Dette er en postprint-versjon/This is a postprint version.
DOI til publisert versjon/DOI to published version: 10.1109/TTHZ.2015.2400224

the figure that the optimum correlation threshold is about 0.25 for the spectral characteristics $\mathbf{K}_2$ and $\mathbf{K}_3$, while a much higher correlation threshold of about 0.85 is optimal for the spectral characteristic $\mathbf{S}$. We also note that the blue curve in Fig. 6(b), corresponding to the $\mathbf{K}_3$ characteristic, is broader, suggesting less sensitivity to the choice of the actual threshold value than for the other characteristics considered here. Figure 6(c) plots the correlation value in each pixel using the best spectral characteristic, $\mathbf{K}_3$. We observe from the figure that the correlation is somewhat lower for the (1%, 4 mm) sample (position 3) and for the sample containing unground tartaric acid (position 6), compared to the other tartaric acid samples. This is not unexpected, because a low tartaric acid fraction (position 3) leads to noisier absorption peaks, while unground tartaric acid (position 6) leads to more scattering.

B. Covered samples

TABLE II
SAMPLES FOR MEASUREMENTS WITH CLOTH BARRIER

Sample no.	Mass fraction	Total mass (g)	Thickness (mm)
1	10% tart. acid	6.1	4.0
2	10% lactose	6.4	4.2
3	10% RDX	5.5	3.5
4	5% tart. acid, 5% lactose	6.5	4.2
5	5% RDX, 5% tart. acid	5.7	3.5
6	5% RDX, 5% lactose	5.8	3.5

Measurements of samples covered by a barrier consisting of one layer of 1.0 mm-thick cloth were also carried out. The samples in this case contained RDX, lactose, and tartaric acid, and mixtures of two of these substances, as shown in Table II. The absorbance of the reference samples for the spectral correlation calculations are shown in Fig. 5(b), together with the absorbance of the cloth barrier.

Figure 7 shows application of SAM to identify the samples containing RDX. Similarly to the case with uncovered samples, we generate ROC curves for the different spectral characteristics. The results are shown in Fig. 7(a). We observe that in the limit of low false positive rate, the spectral characteristic $\mathbf{K}_3$ is superior to the two other characteristics, which was also the result for the measurements on the uncovered tartaric acid samples in Sec. IV-A. Figure 7(b) shows that the optimal correlation thresholds are different, compared to Fig. 6, for all three spectral characteristics. For the spectral characteristic $\mathbf{K}_3$ a correlation threshold of about 0.35 is optimal in this case. The observation that the optimal correlation threshold depends on measurement conditions means that one must either use a low correlation threshold to ensure that the fraction of true positive pixels is high, at the expense of increased false positive rate, or must use a high correlation threshold to ensure that the false positive rate remains low, at the expense of decreased true positive rate. Which of the two strategies is optimal depends on the application. Figure 7(c) shows a spectral correlation image produced using the metric $\mathbf{K}_3$. The structure of the cloth appears as the wavy horizontal lines in the image. The three samples containing RDX distinguish themselves from the

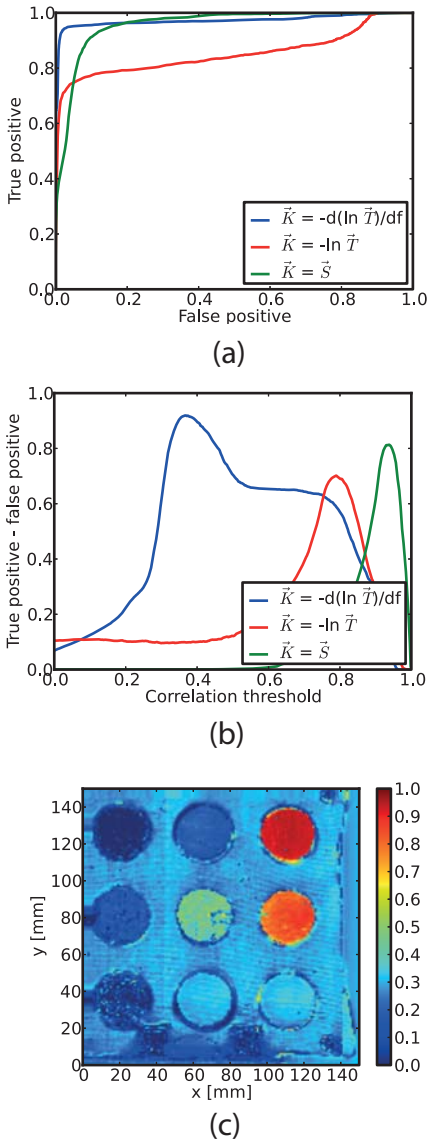

Fig. 7. Testing for RDX, covered samples. (a) ROC curves for the three spectral characteristics for a THz image (transmission mode) of six samples containing tartaric acid, lactose, and RDX, and three reference samples. (b) Identifying the optimal identification threshold. (c) A spectral correlation image using the spectral characteristic $\mathbf{K}_3$.

other samples suggesting both good detectivity and specificity. Clearly, the sample containing RDX only is best identified, followed by the one mixed with lactose. The sample mixed with tartaric acid correlates a bit less with the "pure" RDX spectrum. Looking at Fig. 5(b) we observe that the spectral features of RDX and lactose are better separated than the ones of RDX and tartaric acid. This may explain the observed differences in correlation: the RDX spectrum is less disturbed by the lactose than by the tartaric acid.

Figure 8 shows application of SAM to identify tartaric acid for the covered samples. The figure is based on the same experimental data as in Fig. 7, but the reference spectrum is tartaric acid, instead of RDX. From Fig. 8, we note several points. First, the optimal correlation threshold is lower (about

Dette er en postprint-versjon/This is a postprint version.
DOI til publisert versjon/DOI to published version: 10.1109/TTHZ.2015.2400224

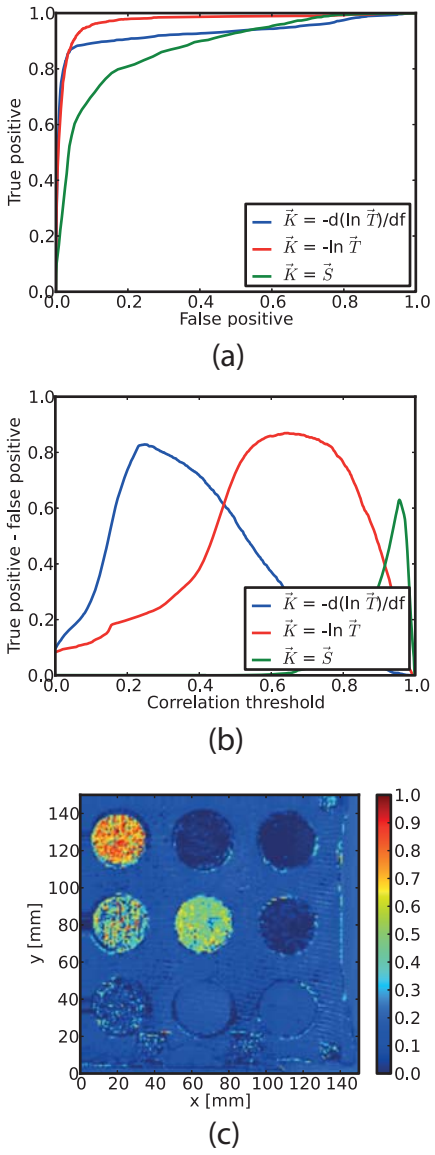

Fig. 8. Testing for tartaric acid, covered samples. a) ROC curves. (b) Identifying the optimal identification threshold. (c) A spectral correlation image using the spectral characteristic $\mathbf{K}_3$.

0.25) for the spectral characteristic $\mathbf{K}_3$, compared to the spectral characteristic $\mathbf{K}_2$ (about 0.65). This is due to the higher specificity of $\mathbf{K}_3$, compared to $\mathbf{K}_2$, as discussed in Sec. II. Second, we observe from Fig. 8(c) that the correlation is low for some of the positive pixels, especially for sample no. 4 containing a mixture of tartaric acid and lactose. The reason for this is that the derivative is sensitive to sharp spectral features. Thus, the presence of the sharp absorption feature of lactose reduces the effect of the absorption feature of tartaric acid when normalizing the spectra. While $\mathbf{K}_2$ has poorer specificity than $\mathbf{K}_3$, it is less sensitive to sharp spectral features, and therefore performs comparable to $\mathbf{K}_3$ in this case, as shown in Fig. 8(b).

V. Conclusion

In conclusion, we have used ROC curves to compare three potential spectral characteristics for use in spectral angle mapping. By measuring on covered and uncovered samples of varying thickness, consisting of pure and mixed materials, we identify the first derivative of the absorption spectrum as a better overall metric, compared to the absorption spectrum or the raw transmission spectrum, although the absorption spectrum shows comparable performance for some combinations of samples and barriers. Furthermore, only a single reference spectrum is needed for each material in the spectral database. This approach might find uses within application of THz transmission spectroscopy for identification of dangerous or illegal substances, for example by assisting a human operator in the interpretation of THz transmission images.

References

[1] K. Kawase, Y. Ogawa, and Y. Watanabe, "Non-destructive terahertz imaging of illicit drugs using spectral fingerprints," *Opt. Express*, vol. 11, pp. 2549–2554, Sep. 2003.

[2] J. R. Schott, *Remote Sensing: The Image Chain Approach*. New York: Oxford University Press, 2007.

[3] A. D. van Rheenen and M. W. Haakestad, "Terahertz imaging spectroscopy - towards robust identification of concealed dangerous substances," in *39th Int. Conf. on Infrared, Millimeter, and THz Waves*, Tucson, Arizona, USA, Sep. 2014.

[4] W. L. Chan, J. Deibel, and D. M. Mittleman, "Imaging with terahertz radiation," *Rep. Prog. Phys.*, vol. 70, pp. 1325–1379, Jul. 2007.

[5] D. Brigada and X.-C. Zhang, "Chemical identification with information-weighted Terahertz spectrometry," *IEEE Transactions on Terahertz Science and Technology*, vol. 2, pp. 107–112, Jan. 2012.

[6] M. Tonouchi, "Cutting-edge terahertz technology," *Nature Photonics*, vol. 1, pp. 97–105, Feb. 2007.

[7] J. El Haddad, B. Bousquet, L. Canioni, and P. Mounaix, "Review in terahertz spectral analysis," *TRAC - Trends in analytical chemistry*, vol. 44, pp. 98–105, 2013.

[8] B. Fischer, M. Hoffmann, H. Helm, G. Modjesch, and P. Uhd Jepsen, "Chemical recognition in terahertz time-domain spectroscopy and imaging," *Semicond. Sci. Technol.*, vol. 20, pp. S246–S253, 2005.

[9] Y. C. Shen, T. Lo, P. F. Taday, B. E. Cole, W. R. Tribe, and M. C. Kemp, "Detection and identification of explosives using terahertz pulsed spectroscopic imaging," *Applied Physics Letters*, vol. 86, 2005, paper no. 241116.

[10] J. Chen, Y. Chen, H. Zhao, G. J. Bastiaans, and X.-C. Zhang, "Absorption coefficients of selected explosives and related compounds in the range of 0.1-2.8 THz," *Optics Express*, vol. 15, pp. 12 060–12 067, Sep. 2007.

[11] F. Ellrich, G. Torosyan, S. Wohnsiedler, S. Bachtler, A. Hachimi, J. Jonuscheit, R. Beigang, F. Platte, K. Nalpantidis, T. Sprenger, and D. Hübsch, "Chemometric tools for analysing terahertz fingerprints in a postscanner," in *37th Int. Conf. on Infrared, Millimeter, and THz Waves*, Wollongong, Australia, Sep. 2012.

[12] F. Platte and H. M. Heise, "Substance identification based on transmission THz spectra using library search," *Journal of Molecular Structure*, vol. 1073, pp. 3–9, 2014.

[13] H. Wu, E. J. Heilweil, A. S. Hussain, and M. A. Khan, "Process analytical technology (pat): Quantification approaches in terahertz spectroscopy for pharmaceutical application," *Journal of Pharmaceutical Sciences*, vol. 97, pp. 970–984, Feb. 2008.

[14] Y. Watanabe, K. Kawase, T. Ikari, H. Ito, Y. Ishikawa, and H. Minamide, "Component analysis of chemical mixtures using terahertz spectroscopic imaging," *Optics Communications*, vol. 234, pp. 125–129, 2004.

[15] M. van Exter, C. Fattinger, and D. Grischkowsky, "Terahertz time-domain spectroscopy of water vapor," *Optics Letters*, vol. 14, pp. 1128–1130, Oct. 1989.

[16] M. C. Kemp, "Explosives detection by terahertz spectroscopy–a bridge too far?" *IEEE Transactions on Terahertz Science and Technology*, vol. 1, pp. 282–292, Sep. 2011.

[17] A. D. van Rheenen and M. W. Haakestad, "Detection and identification of explosives hidden under barrier materials - what are the THz-technology challenges?" *Proc. SPIE*, vol. 8017, p. 801719, 2011.

Dette er en postprint-versjon/This is a postprint version.
DOI til publisert versjon/DOI to published version: 10.1109/TTHZ.2015.2400224

[18] F. Théberge, M. Châteauneuf, J. Dubois, S. Désilets, and L.-S. Lussier, "Spectral artifacts from non-uniform samples analyzed by terahertz time-domain spectroscopy," *Optics Express*, vol. 17, pp. 10 841–10 848, Jun. 2009.
[19] F. Ellrich, T. Weinland, M. Theuer, J. Jonuscheit, and R. Beigang, "Fiber-coupled Terahertz spectroscopy system," *Techn. Messen*, vol. 75, pp. 14–22, 2008.

Arthur D. van Rheenen obtained his PhD in Electrical Engineering (1987) from the University of Florida, Gainesville. From 1980 to 2005 he has published on different aspects of noise in electronic devices. The last 10 years he has been studying and modeling propagation or IR radiation through the atmosphere. In addition, imaging and spectral recognition of dangerous and/or illegal substances using THz technology has been a research theme over the last five years.

Magnus W. Haakestad received a PhD in electrical engineering from the Norwegian University of Science and Technology in 2006. Since then he has been a scientist at the Norwegian Defence Research Establishment. His research interests include infrared laser sources, nonlinear optics, fiber optics, and terahertz technology. He spent one sabbatical year at Edward L. Ginzton Laboratory, Stanford University, where he worked with mid-infrared frequency combs for molecular spectroscopy.

Dette er en postprint-versjon/This is a postprint version.
DOI til publisert versjon/DOI to published version: 10.1109/TTHZ.2015.2400224